Geophys. J. Int. (2004) **157,** 55–63 doi: 10.1111/j.1365-246X.2004.02155.x

Using time- and temperature-dependent Preisach models to investigate the limitations of modelling isothermal remanent magnetization acquisition curves with cumulative log Gaussian functions

D. Heslop,[1] G. McIntosh[2] and M. J. Dekkers[3]

[1] *Fachbereich Geowissenschaften, University Bremen, Postfach* 330440, D-283334 *Bremen, Germany. E-mail: dheslop@uni-bremen.de*
[2] *Department of Geophysics and Meteorology, University of Madrid,* E-28040*, Spain*
[3] *Paleomagnetic Laboratory 'Fort Hoofddijk', Department of Earth Sciences, Utrecht University, Budapestlaan* 17, 3584 *CD Utrecht, the Netherlands*

Accepted 2003 October 7. Received 2003 October 2; in original form 2003 July 2

SUMMARY

A number of recent studies have applied the cumulative log Gaussian (CLG) modelling technique to bulk isothermal remanent magnetization (IRM) curves to investigate the coercivity contributions of different minerals contained within a natural sample. Here, we present a series of Preisach–Néel models used to investigate how robust the assumption of fitting lognormal coercivity distributions is in the presence of local interaction fields and thermal relaxation. Our models indicate that the starting state of the magnetic system, magnetic interaction and thermal relaxation have a strong influence on the form of IRM curve, meaning that in a substantial number of cases the lognormal assumption fails and the CLG procedure can produce misleading interpretations. In some cases the failure of the CLG assumptions produces models which introduce spurious additional coercivity components into the fitted curve.

Key words: IRM acquisition, Preisach model, rock magnetism.

INTRODUCTION

The problem of unmixing natural magnetic assemblages into individual coercivity distributions is complex. Recently, a number of studies have followed the experimental work of Robertson & France (1994) and concentrated on fitting bulk acquisition curves of the isothermal remanent magnetization (IRM) with models that assume that each coercivity population can be represented by a single lognormal distribution. A number of techniques have been developed to perform this unmixing (Stockhausen 1998; Kruiver *et al.* 2001; Heslop *et al.* 2002). Other authors (Egli 2003) have suggested fitting procedures using more adaptable distributions that include additional shape parameters such as kurtosis and skewness. In the previous discussions of cumulative log-Gaussian (CLG) fitting, little attention has been given to considering when the fundamental assumption, that coercivity populations can be represented by lognormal distributions, could fail. An important point that has only been addressed in a general way is the effect of magnetic interactions on the IRM acquisition curve and their subsequent influence on the CLG analysis. Robertson & France (1994) suggested that magnetic interaction (specifically dipole–dipole interaction) would affect the spread of individual coercivity distributions, but for minerals such as magnetite it was expected that this effect would be minimal. Kruiver *et al.* (2001) proposed that the linear additivity of the different lognormal coercivity components would only hold in the absence of interactions, whereas Heslop *et al.* (2002) suggested that no interactions should be present if CLG analysis was to be applied successfully.

Additional factors that could influence IRM acquisition are thermal relaxation and the starting state of the magnetic system. These two points were not addressed in any of the above studies, however Petrovský *et al.* (1993) have shown that remanence based measurements performed on synthetic haematites were influenced by starting state. In addition, Thamm & Hesse (1998) performed calculations that demonstrated that the remanence acquisition properties of an ensemble of Stoner–Wohlfarth particles would be strongly controlled by initial demagnetization processes.

Here, we utilize a Preisach–Néel model for Stoner–Wohlfarth grains (Spinu & Stancu 1998; Stancu 1998; Spinu *et al.* 2001; Borcia *et al.* 2002) to study the effects that local field interactions, thermal relaxation, and the starting state of the magnetic system have on the CLG analysis of a single lognormal coercivity distribution. We investigate deviations from lognormal behaviour, which can cause the coercivity distribution to be skewed, making mineral identification less straightforward. Also, a single coercivity distribution may appear as though it should be modelled with two lognormal components, supporting the results of Egli (2003).

THE PREISACH–NÉEL MODEL

The classical Preisach model (Preisach 1935; Néel 1954) utilizes populations of hysterons to explain the hysteresis behaviour

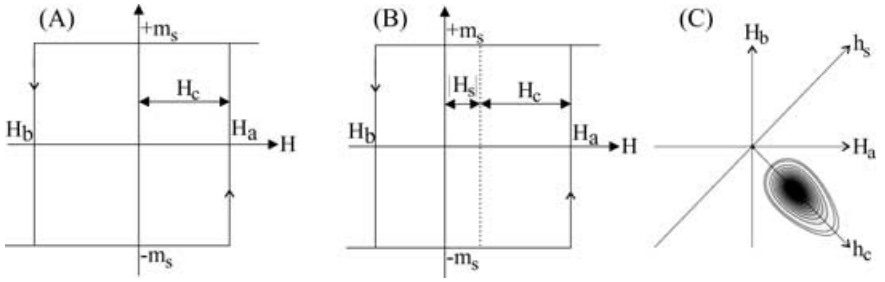

Figure 1. (a) and (b) Elementary Preisach hysteresis loops with switching fields H_a and H_b. The loop in (a) contains no local interaction field, therefore $H_a = -H_b = H_c$, whereas the loop in (b) includes a local interaction field, therefore $H_a \neq -H_b \neq H_c$. (c) The Preisach plane, all points in the half-plane $a \geq -b$ correspond to hysterons with up and down switching fields of H_a and H_b respectively, whilst points in the half-plane $b > a$ represent reversible cycles and are therefore not important when considering remanences (Dunlop *et al.* 1990). (c) shows an example of a Preisach distribution function, which represents the number of hysterons occurring in the different parts of the half-plane. This representation utilizes a different coordinate system (h_a, h_s) to the (H_a, H_b) system used in (a) and (b), which requires a 45° rotation, i.e. $h_c = H_c\sqrt{2} = (H_a - H_b)/\sqrt{2}$ and $H_s = h_s\sqrt{2} = (H_a + H_b)/\sqrt{2}$.

of an ensemble of particles. The hysteron is a square hysteresis loop (Fig. 1a) representing a single-domain particle with uniaxial anisotropy with a coercivity of $\pm H_c$ and possible magnetization states $\pm m_s$. If a local interaction field, H_s, is introduced the hysteron becomes asymmetric about the zero field point and has ascending and descending switching fields defined as $H_a = H_c + H_s$ and $H_b = -H_c + H_s$ respectively (Fig. 1b). The distribution of hysterons, $p(H_a, H_b)$, at any point in the half-plane $a \geq -b$ is called the Preisach distribution (Fig. 1c). The magnetization of the system, M, is then given by the integral over the $a \geq -b$ half-plane:

$$M = \int_{S^+} p(H_a, H_b)\, dH_b\, dH_a - \int_{S^-} p(H_a, H_b)\, dH_b\, dH_a \qquad (1)$$

where S^+ represents hysterons with a magnetization in the up position and S^- represents hysterons with a magnetization in the down position (Hejda *et al.* 1994). Hysterons located on the $a = -b$-axis are non-interacting and a condition of the model is that the Preisach distribution is symmetrical about this diagonal. Thus, the coercivity spectrum of the Preisach distribution in the absence of local interaction fields can be obtained by profiling along $a = -b$ and the distribution of local interaction fields can be found by profiling perpendicular to $a = -b$ (Dunlop *et al.* 1990; Hejda & Zelinka 1990). The traditional interpretation of the Preisach diagram is that the off-diagonal part of the distribution represents the spectrum of magnetostatic particle interactions contained within a sample. The Preisach model is however phenomenological; therefore it is not possible to define an exact relationship between the local field interactions utilized in the Preisach model and the interactions observed in real systems. An additional form of interaction can be introduced to the Preisach model in the form of a magnetization-dependent mean field term, which assumes that to a first-order the magnitude of interactions is proportional to the magnetization of the system (Della Torre 1966). For simplicity, we do not consider mean field interactions in the majority of our models, however, a brief discussion on their influence is given below. Using the Preisach approach it is possible to simulate a number of starting states for a magnetic system. In this study we are interested in two main starting states:

(1) The virgin state: all the hysterons in the fourth quadrant of the Preisach plane (i.e. those capable of carrying a stable remanence) have an equal probability of being in either the up or the down magnetization state (Fig. 2a). This is equivalent to a fully thermally demagnetized system.

(2) The static alternating current (AC) demagnetized state: the Preisach distribution becomes polarized about the $a = -b$-axis, hysterons with a positive (negative) local interaction field are magnetized in the down (up) direction (Fig. 2b).

The starting state of the system is an important consideration in magnetic studies. IRM component analysis can be performed on either the forward IRM acquisition curve or alternatively on the backward direct current (DC) demagnetization curve (when the sample is taken from positive to negative saturation). Here we will only consider forward IRM acquisition curves because in the absence of a mean field term the forward IRM curve from a virgin state in the Preisach model is equivalent to the DC demagnetization curve (it is however important to emphasize that this equality would not exist

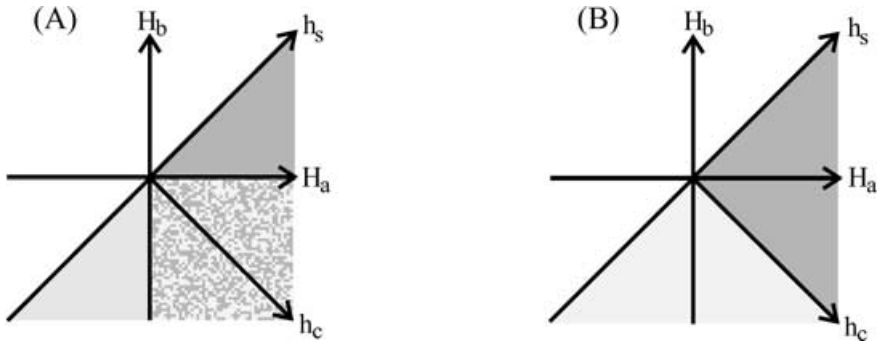

Figure 2. (a) and (b) Initial magnetic states represented in the Preisach plane. In (a) a virgin state is shown, where all the hysterons in the fourth quadrant have an equal probability of being magnetized in the positive (light shading) or negative (dark shading) direction. An AC demagnetized state is shown in (b) where the Preisach plane becomes polarized about the $a = -b$-axis.

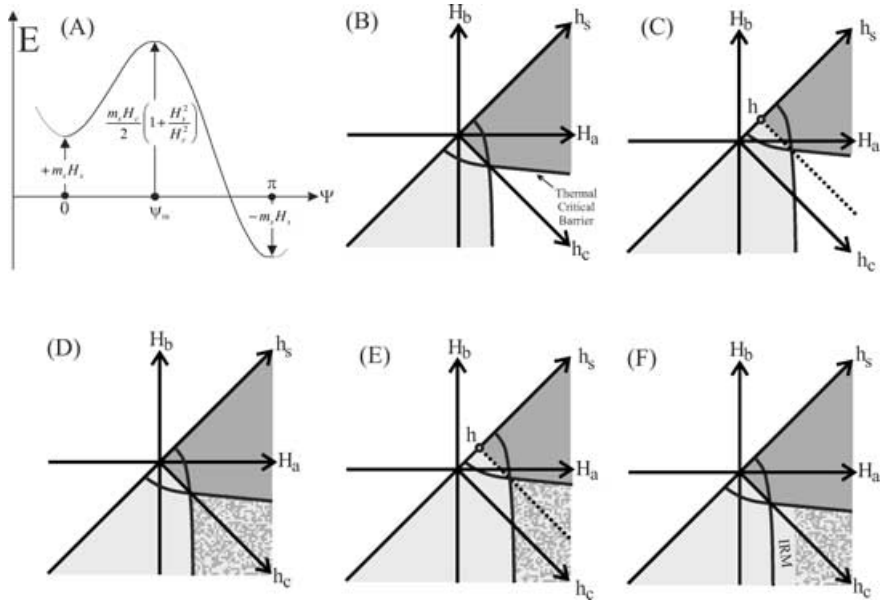

Figure 3. (a) The double-well potential for a Stoner–Wohlfarth grain, based on Spinu & Stancu (1998). The angle between the easy-axis of the grain and the applied field is given by ψ. Nonlinear thermal critical barriers for Stoner–Wohlfarth grains with their easy axes parallel to the applied field direction using the interpolation expression of Pfeiffer (1990) are shown in (b) and (c). Light (dark) shading represents hysterons with an up (down) magnetization in the current model conditions (i.e. as a function of applied field, temperature, and time); regions of the diagram with no shading show the hysterons which do not undergo relaxation. (b) represents model conditions in zero field and (c) in an applied external field of magnitude H in the (H_a, H_b) coordinate system and $h = H\sqrt{2}$ (this position is unaffected by the interaction field of the hysterons because in all our models we assume that the mean field interaction term is equal to zero). (d), (e) and (f) show the process of IRM acquisition in the Preisach–Néel model with (d) starting from the virgin state, (e) application of an applied field, (f) removal of the field and the resulting remanence (IRM) in the up direction.

for natural samples). In the virgin state, half of the hysterons will be in the up state and half will be in the down state; during IRM acquisition only the down state hysterons will change their magnetization. Because the down state hysterons are distributed randomly throughout the Preisach distribution, they will provide a full representation of the coercivity spectrum and local field interaction terms during acquisition. The DC demagnetization curve is therefore simply an inverted version of the IRM curve with twice the magnitude.

In this form, the so-called classical Preisach model does not allow for thermal relaxation of the magnetic system. Here, we adopt the Preisach–Néel model, which includes thermally induced flips in the magnetization of the hysterons (Spinu & Stancu 1998; Stancu 1998; Spinu *et al.* 2001; Borcia *et al.* 2002). The double well energy potential is a function of the grains' magnetization, coercivity, interaction field, and the angle of its easy-axis to the applied field (Fig. 3a). This expression of the grains energy reveals two energy minima (known as wells), corresponding to the two stable equilibrium orientations of the magnetization. The energy curve demonstrates that a hysteron requires sufficient thermal activation to overcome the critical energy barriers before relaxation can occur (Stancu 1998) when H is smaller than the switching field of a hysteron without thermal activation. Through thermal activation, the system will initially pass over the lower of the two energy barriers. However, if the level of thermal activation is sufficient to overcome both barriers, the system will adopt the lower of the two energy states available. As temperature, or time, is increased more grains will relax into their equilibrium magnetization state. For specific model conditions of applied field and temperature it is possible to use the double-well potential to determine which grains will undergo relaxation. The boundaries in the Preisach plane that separate the relaxing grains from the thermally stable grains are termed the thermal critical barriers. In our study we utilize interpolated thermal critical barriers based on the expression of Pfeiffer (1990) for Stoner–Wohlfarth grains (Stoner & Wohlfarth 1948) with their easy-axis not necessarily aligned with the applied field, H:

$$h_t = \frac{h_c}{2}\frac{H_k}{H_c(\psi)}\left(1 \pm \frac{h - h_s}{h_c}\right)^{g(\psi)} \tag{2}$$

with

$$g(\psi) = 0.86 + 1.14\frac{H_c(\psi)}{H_k} \tag{3}$$

and

$$H_c(\psi) = H_k(\sin^{2/3}\psi + \cos^{2/3}\psi)^{-3/2} \tag{4}$$

where ψ is the angle between the easy-axis of the grain and the applied field; H_k is the anisotropy field and h_c is the critical field at which the magnetization of the grain will switch in the (h_c, h_s) coordinate system. For specific conditions a critical h_t (a function of temperature and time) is set enabling h_t to be calculated for each grain to determine whether it will relax within the given conditions of the measurement process. As h_t increases, the thermal critical barrier separating relaxing and stable grains propagates further into the Preisach plane along an axis that is determined by the magnitude of h (cf. Figs 3b and c). Figs 3(d), (e) and (f) show the process of IRM acquisition starting from a virgin state. After application and removal of the applied field, h, a region of the fourth quadrant of the diagram becomes magnetized in the up state forming an IRM.

MODELLING PROCEDURE

For each model, a Preisach distribution of 10^4 hysterons was generated whose properties were controlled by a joint probability

distribution function in the (h_c, h_s) coordinate system, with log-normally distributed critical fields and normally distributed local interaction fields according to the equation:

$$p(h_c, h_s) = \frac{1}{2\pi s_s s_c} \exp\left[-\frac{\log(h_c - \overline{h_c})^2}{2s_c^2}\right] \cdot \exp\left[-\frac{h_s^2}{2s_s^2}\right] \quad (5)$$

where $\overline{h_c}$ is the mean of the distribution of critical fields, s_c is the standard deviation of log coercivities and s_s is the standard deviation of the distribution of local interaction fields (with zero mean). This distribution was adopted for reasons of simplicity however, recent results from first-order reversal curve (FORC) analysis has shown that many other distributions can be present in natural samples (Roberts *et al.* 2000), and theoretical investigations indicate that in an ensemble of randomly orientated, randomly distributed magnetic moments, the magnetostatic interactions will follow a Cauchy distribution (Shcherbakov & Shcherbakova 1975).

Recent models have considered the possibility that the form of the Preisach distribution can change as a function of the magnetic state of the sample, for example the variable variance Preisach-Néel model which employs a link between the number of superparamagnetic particles in the system and the variance of the interaction field distribution (Borcia & Spinu 2002). For simplicity we consider the form of Preisach distribution utilized in our models to be independent of the state of the magnetic system.

For all the models the same distribution of critical fields was used with $\overline{h_c} = 15$ mT and $s_c = 0.1$. Individual models were executed for a specific relaxation term (H_t, where $h_t = H_t\sqrt{2}$). The procedure of each model initially involved defining the magnetization directions of the hysterons to give the desired starting state. IRM acquisition was simulated in 1 mT increments to a saturation field: in this case a field of 40 mT was found to be sufficient to reach a saturation state in all the models and a typical IRM curve would take *ca* 30 s to calculate. Each applied field increment consisted of two modelling steps, application of the field and then assessment of the remanent magnetization in a zero field. It would be possible to model the acquisition procedure with different H_t values for the in-field and measurement steps of the model (which would provide a more realistic representation of the real laboratory situation), however, since these values would be equipment/operator dependent, H_t was assumed to be identical for the in-field and zero field (measurement) parts of the model.

RESULTS

First, we present the results of two collections of models for both virgin and AC demagnetized states:

(1) Simulating thermal relaxation in non-interacting particle systems.
(2) Simulating interacting particle systems with zero thermal activation.

The resulting IRM curves were analysed using a two-component CLG model fitted using the expectation-maximization approach of Heslop *et al.* (2002). In this modelling experiment, the IRM curve should consist of a single coercivity component. Therefore, the relative proportion of a potentially present second CLG component required to obtain a good fit of the model to the data is taken as a measure of the deviation of the curve from lognormality.

A NON-INTERACTING MODEL WITH THERMAL RELAXATION

In the first set of models we remove the local field interaction term, i.e. $s_s = 0$ mT, in order that all the hysterons lie on the $a = -b$-diagonal, and investigate the effects of thermal relaxation on the CLG analysis with $0 \leq H_t \leq 2.5$. To provide an impression of what H_t means in terms of which grains will relax in the given models, the value can be related to non-interacting grains aligned in zero applied field by the following equation (*cf.* Stancu 1998):

$$\frac{H_k}{2} = H_t \quad (6)$$

Therefore, grains that meet the above conditions with $H_k \leq 5$ mT would undergo relaxation in the models that utilize H_t at its maximum value of 2.5. Using the approximation given by Dunlop & Özdemir (1997) to find the blocking volume of a grain (V_B) at a temperature T:

$$V_B \approx \frac{50kT}{\mu_0 M_s H_K} \quad (7)$$

We find that at room temperature grains which are aligned with the applied field and have a diameter $< \sim$50 nm will undergo relaxation when H_t is at its maximum value of 2.5. Figs 4(a) and (b) show the two end-members for samples with a virgin starting state. For the non-interacting, non-relaxing model the calculated IRM curve is almost identical to the pre-defined coercivity distribution, and this curve should be fitted with a single component CLG model (the second component shown in the figure makes less than a 2 per cent contribution to the bulk model). At the alternative extreme when H_t is set to 2.5, a very different IRM curve is produced. First, the curve does not coincide with the coercivity distribution because as expected for a relaxing system it is shifted to lower coercivities. Secondly, it is necessary to fit a two-component CLG model to the curve to obtain a good fit. When the model is set to a fully AC demagnetized starting state a similar pattern is observed to that for the virgin samples (Figs 4c and d). For the AC demagnetized non-relaxing model a single lognormal component is observed in the IRM curve (in this case the fitted second component makes less than a 0.5 per cent contribution to the bulk model), which provides a close match to the defined coercivity distribution. A shift to lower coercivities is again seen for the relaxing model and the necessity for a two-component CLG model is clear.

As a proxy for the deviation from lognormal behaviour we have plotted the proportion the dominant component makes to the bulk two-component CLG model for the IRM curves as the effect of thermal relaxation is increased (Fig. 4e). For virgin samples it appears that the deviation from a single-component model is approximately linear with respect to thermal relaxation. For the AC demagnetized system a different pattern is observed where a single component dominates until $H_t = \sim$0.75, then the contribution decreases linearly with increasing H_t. This behaviour is expected within the conditions of the model and the scatter of the points about the central trend is believed to be mainly due to the expectation-maximization fitting routine which can produce quite variable results for multi-component systems where major and minor components are almost completely overlapping. When considering thermal activation the hysterons that will relax most readily are those with the lowest coercivity and include a negative local interaction field. However, in the AC demagnetized state these hysterons are already magnetized in the up direction and the lowest energy state available to them is also in the positive direction, so their direction of magnetization

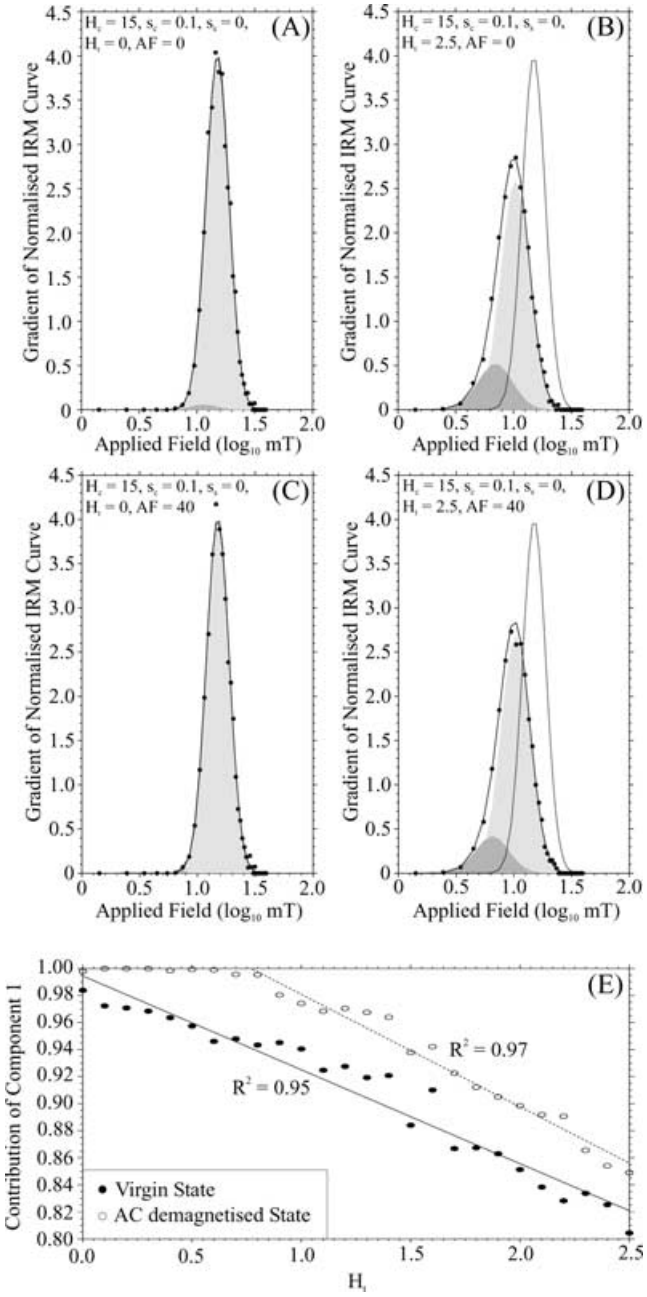

Figure 4. CLG models for a non-interacting, thermally relaxing system. Data points from the modelled IRM curve and the predefined coercivity distribution are shown as filled circles and a dashed line respectively. The two fitted CLG components are shown as shaded regions and the bulk model is displayed as a full line. Plots (a) and (b) show the CLG models for models starting from a virgin state with H_t of 0 and 2.5 respectively. (c) and (d) show the same models started from a AC demagnetized state. In (e) the relative contribution of the dominant component in the CLG models is taken as a good approximation for the deviation of the IRM curve from a lognormal distribution. Linear trend lines and correlation coefficients are given for the portions of plot where relative contribution of the dominant component is decreasing.

remains unaffected by thermal activation. It is only once thermal relaxation has passed a certain threshold, that the hysterons with positive local interaction fields are affected and thermal activation is actually observed, in this case once $H_t \geq \sim 0.75$. In the virgin state the hysterons have no preferred magnetization direction so the low-coercivity grains with negative local interaction fields can initially be magnetized in the down direction and then readily flip their magnetization under low-level thermal activation. This principally explains the difference in the behaviour observed for different starting states in Fig. 4.

This collection of models demonstrates some important points. First, the magnetic starting state plays an important role in determining the IRM acquisition curve and therefore also the final CLG model. Secondly, even under the strictest criterion for the application of a CLG model (i.e. complete absence of magnetic interactions), thermal relaxation can cause both shifts in the coercivity distribution to lower values and deform the curve so that it appears to require a two-component CLG model to provide a robust fit. A similar result showing the time-dependency of IRMs in single-domain magnetites was obtained experimentally by Worm (1999), who found that for low fields the IRM produced in a sample held in field for 10 s was approximately three times greater than for the same sample held in field for 0.01 s. This was in contrast to higher field measurements where there was a negligible difference in the IRMs produced by the short and long field applications. This demonstrates the region of the coercivity spectrum that contains soft grains will be more strongly affected by thermal relaxation and this would produce the pattern of negative skewness that is observed in our models. A number of previous studies that have performed CLG analysis upon IRM curves obtained from natural samples have utilized two model components to fit a negatively skew distributions of the type obtained in our models using a single relaxing coercivity component (Eyre 1996; Kruiver & Passier 2001; Heslop *et al.* 2002).

LOCAL FIELD INTERACTION WITH ZERO THERMAL RELAXATION

To study the effect of local field interaction on the CLG models we present a collection of models with $0 \leq s_s \leq 5$ mT for both virgin and AC demagnetized initial states. Although this interaction field may appear high with respect to the coercivity distribution (representing $\frac{1}{3}$ of the mean coercivity) we select this value for a number of reasons. First, it represents an end-member value and lower interaction fields will also be considered. Secondly, recent evidence obtained from FORC diagrams demonstrates that many natural samples may have interaction fields with a magnitude up to one third of their mean coercivity [if the interaction is interpreted as existing between single-domain particles, Roberts *et al.* (2000)]. Finally, for a collection of homogeneously dispersed, randomly orientated single-domain grains Shcherbakov & Shcherbakova (1975) showed that the probability distribution of the interaction fields, H_s, is given by the Cauchy distribution:

$$p(H_s) = \frac{1}{\pi b \left[1 + \left(\frac{H_s - H_0}{b}\right)^2\right]} \tag{8}$$

where H_0 is the demagnetizing field (zero in the presented model), and $b = 8\pi^2 M_{rs}/9\sqrt{3}$ (where M_{rs} is equal to the product of the mean magnetic moment of the grains and their volume concentration, i.e. the saturation remanence of the particles in the absence of interactions). For a system of Stoner–Wohlfarth grains, M_{rs} is given by $M_s/2$ and at a typical magnetite volume concentration for a natural sample (1 per cent) we obtain $\mu_0 b = 15.3$ mT. In this case the b term is the scale parameter of the Cauchy distribution and is considered to represent the typical strength of the local interaction field. This would indicate that for single-domain (SD) magnetite assemblages at concentrations typical of natural samples local field interactions

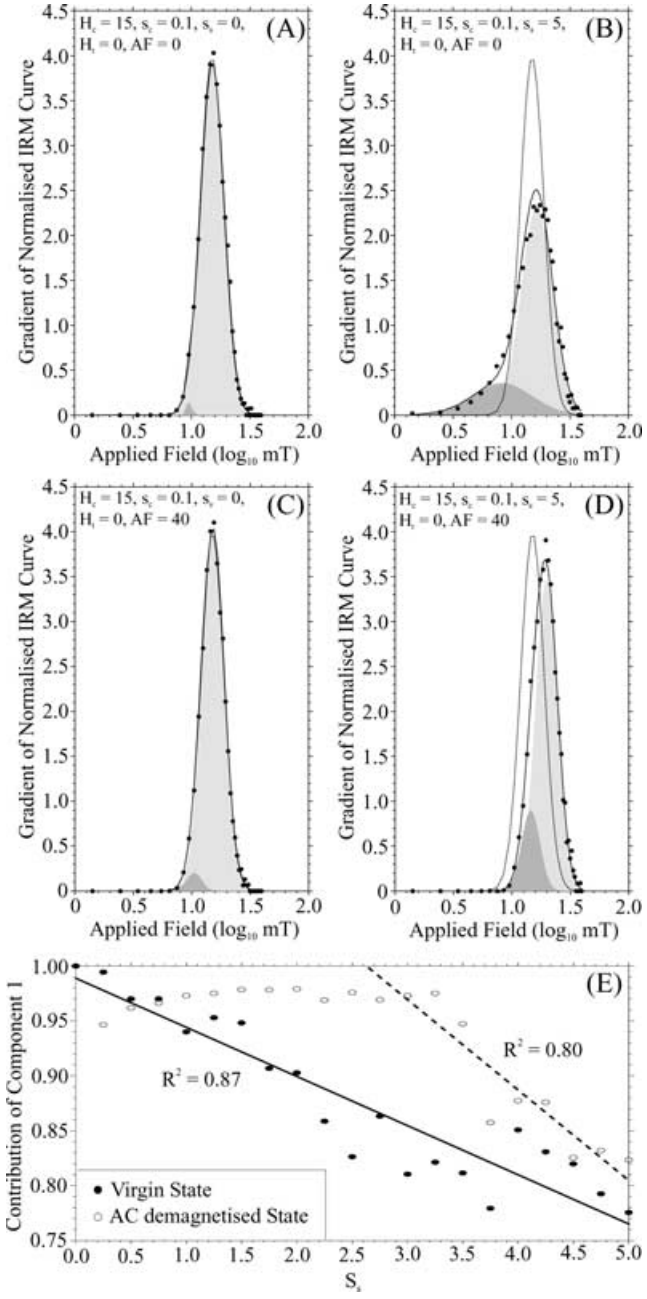

Figure 5. CLG models for a non-relaxing system that includes local interaction field terms. The plots are the same format as that used in Fig. 4 with s_s values of 0 and 5 mT.

can be present which are substantially greater than those utilized in our $s_s = 5$ mT model.

For the end-member model with $s_s = 0$ mT an IRM curve is produced in the virgin system which is essentially identical to the predefined coercivity distribution (Fig. 5a). In practise this curve would be fitted with a single CLG component (here the shown second component makes <5 per cent contribution). For $s_s = 5$ mT the distribution is clearly no longer lognormal and a substantial second component is required to fit data (Fig. 5b). This diagram shows that upon the introduction of interaction fields, the IRM acquisition curve for an assemblage of grains with a virgin starting state becomes negatively skewed and is shifted towards lower coercivities (i.e. it becomes softer).

For the static AC demagnetized starting state a different pattern is observed in the $s_s = 5$ mT model (Fig. 5d). Here, the distribution has become very slightly negatively skewed but has shifted to higher coercivities. This shift can be explained using Preisach theory. As previously discussed, in the AC demagnetized state the Preisach distribution is polarized about the $a = -b$-axis with only the hysterons with positive local interaction fields i.e. $a > -b$ magnetized in a down state. It is the flipping of the magnetization of these hysterons that will produce the forward IRM acquisition and because they all have positive mean field terms they will produce a curve that is shifted to higher coercivities. The extent of the skewness of the distribution is also less in the AC demagnetized state than the virgin state, again this can be explained by Preisach theory. In log space the shift in coercivity resulting from the introduction of a local interaction field will be greater for a negative interaction field than for a positive interaction field of the same magnitude.

When considering the behaviour of all the models in this group, the pattern that emerges as a consequence of interaction is one of apparent two-component models (Fig. 5e), which is similar to that for non-interacting models with thermal relaxation included (Fig. 4e). For the virgin starting state the decrease of the contribution is approximately linear with respect to increasing s_s, whereas for the AC demagnetized starting state the decrease is only observed after $s_s >$ ~3.0 mT.

VARYING LOCAL INTERACTION FIELD AND THERMAL RELAXATION

Models that include both interaction and relaxation give results that are a combination of the behaviour of the models discussed above. To analyse the IRM curves produced by the various models we used two different methods. First, the difference between the modelled IRM curve and the cumulative distribution function of the predefined coercivity distribution was assessed using the sum of squared residuals. Secondly, the area under the curve of the first derivative of the IRM in the $\log_{10}$ space was populated with 10^4 random numbers to provide a sample that could be used in the Lilliefors test (Conover 1980). The Lilliefors test assesses the goodness of fit of a normal distribution of unspecified mean and standard deviation to

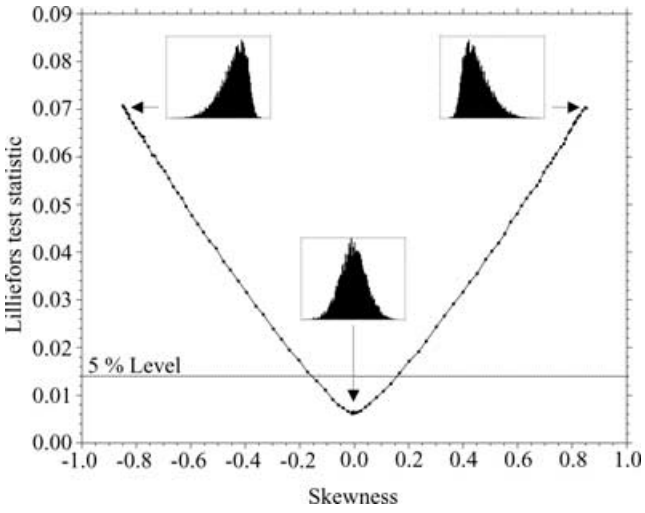

Figure 6. Investigation of the Lilliefors test for skewed distributions. The Lilliefors test statistic was calculated for distributions with different levels of skewness and it was found that a sample of 10^4 points could be considered (at the 5 per cent significance level) as being normally distributed if the test statistic was ≤ 0.014.

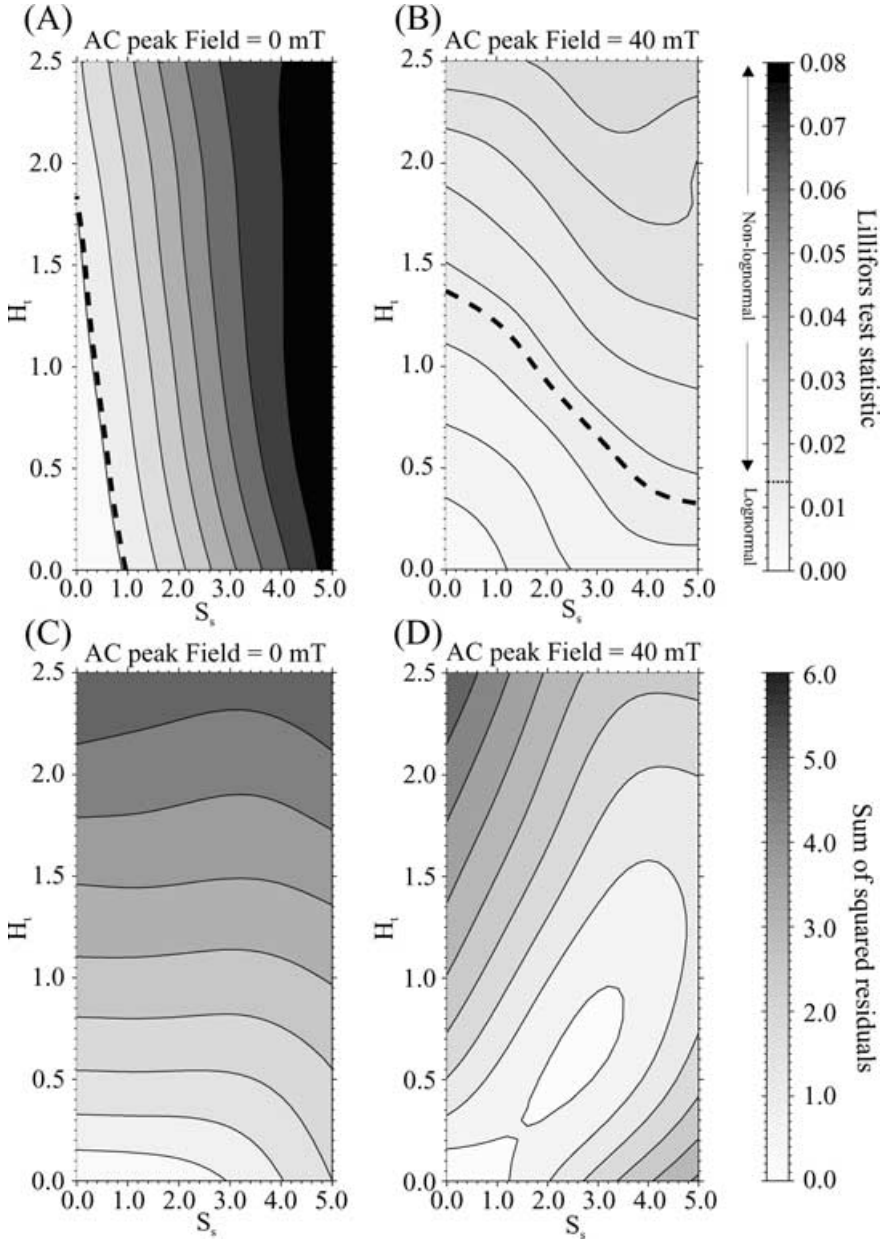

Figure 7. Maps of the properties of IRM curves as a function of local interaction fields and thermal relaxation terms. (a) and (b) show the results of the Lilliefors test for virgin and AC demagnetized samples, the thick dashed line shows the cut-off value of the test statistic (0.014). Above this value the distribution is assumed to be not normally distributed at the 5 per cent level. Plots (c) and (d) assess the difference between the IRM acquisition curve and the predefined coercivity distribution using the sum of squared residuals. This demonstrates that for some samples which pass the Lilliefors test and could therefore be modelled with a single CLG component, the resulting fit would differ greatly from the actual coercivity distribution of the magnetic assemblage.

the data. The test compares the empirical distribution of the modelled IRM curve with a normal distribution having the same mean and standard deviation. Here we use the value of the test statistic to assess the normality of the IRM curve. For comparison the test statistic was calculated for a number of skew-normal distributions (Azzalini 1985). Numerically we determined that a sample of 10^4 random numbers taken from a skew-normal distribution would fail the Lilliefors test (at the 5 per cent significance level, Fig. 6) when the test statistic rose above *ca* 0.014, corresponding to values of skewness greater than ± 0.155.

The results of the models demonstrate the importance of the starting state of the magnetic system on subsequent IRM acquisition. For the virgin starting state, only a small proportion of the models pass the Lilliefors test for normality (Fig. 7a) demonstrating that the assumption of lognormality fails for most states of local field interaction and thermal relaxation. Starting from the AC demagnetized state a much smaller range of values are found and a greater proportion of the models pass the Lilliefors test (Fig. 7b). The reason for this difference is the same as that discussed earlier: in the AC demagnetized state only hysterons with positive local interaction fields are involved in the acquisition procedure, whereas hysterons with both negative and positive local interaction fields are included in the virgin state resulting in a greater skewing of the coercivity distribution in log space.

These results are complemented by the sum of squared residuals (SSR), (Figs 7c and d), which were calculated to assess the

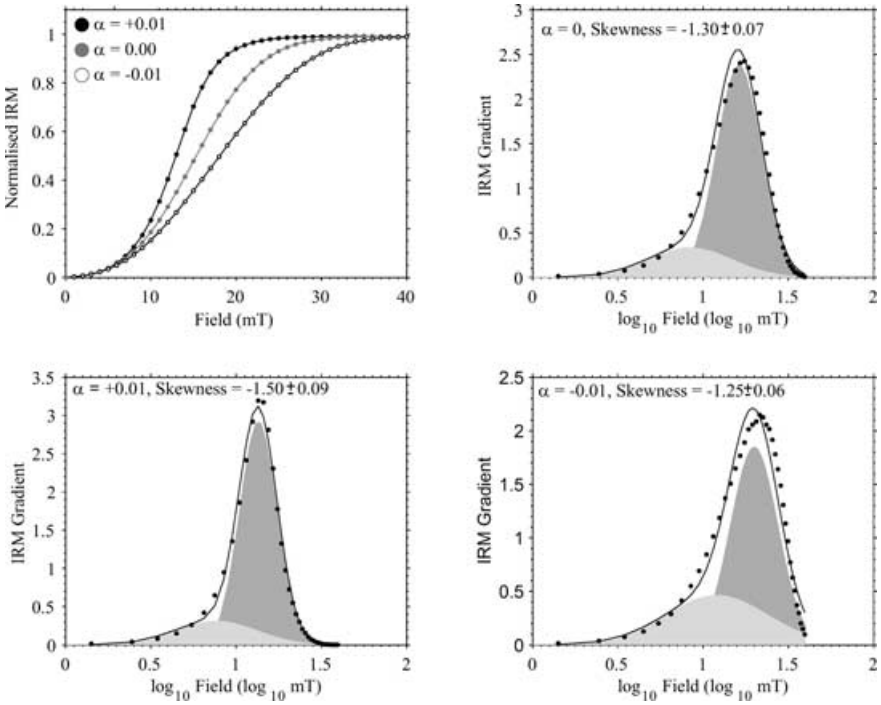

Figure 8. Preliminary investigation of the influence of a mean field interaction term (α) on the form of the IRM curves produced by the Preisach–Néel model. All three models require a two-component fit and the skewness of the distribution is clearly influenced by α, with reduced skewness for a negative term and increased negative skewness for a positive term.

difference between the modelled IRM curve (i.e. the measured coercivity distribution) and the true coercivity distribution (defined in the Preisach–Néel model). Where SSR values are larger, the measured coercivity distributions shows a greater deviation from the true coercivity distribution. By comparing these values to the values for the Lilliefors test it is found that in some regions where the measured coercivity distribution is lognormal, therefore appearing to meet the criterion of CLG fitting, the values of the coercivities are substantially different to those of the true distribution. As with the Lilliefors test, the starting state of the magnetic system plays an important role in controlling how closely the resulting IRM curve matches the coercivity distribution of the Preisach model.

Here, we also took the opportunity to perform a preliminary investigation into the influence of the introduction of a mean field term, α, into our models (Della Torre 1966). This term is magnetization-dependent and is used to calculate an effective field with which the system is magnetized according to:

$$H_{\text{eff}} = H + \alpha M \tag{9}$$

We compared the skewness of three IRM acquisition curves starting from a virgin state with no thermal activation, local field interactions of $s_s = 5$ mT and values of α of -0.01, 0.00 and 0.01 (Fig. 8). All three of the curves are negatively skewed and require a two-component interpretation to produce an adequate fit of the Gaussian model to the data points. This demonstrates that if the influence of a mean field term is significant in natural magnetic materials, it becomes one more complicating factor in the CLG interpretation of remanence curves.

DISCUSSION AND CONCLUSIONS

Up until now there has been no consensus concerning the criterion under which CLG analysis can be successfully applied to IRM acquisition curves (Heslop *et al.* 2002; Egli 2003). Here we have analysed the effects of thermal relaxation and magnetic interaction in some detail with the help of the Preisach approach. Deviations from lognormality can be rather substantial.

The influence of the starting state is essential: the AC demagnetized state should be preferred. In this respect all IRM curves we have analysed so far (Kruiver & Passier 2001; Heslop *et al.* 2002; Kruiver *et al.* 2002; van Oorschot *et al.* 2002; Grygar *et al.* 2003; Kruiver *et al.* 2003) were in the AC demagnetized starting state, fortunately the state where the lognormality criterion is least violated. The use of the AC demagnetized starting state for IRM acquisition appears to be an attractive option, however, consideration must be given to the AC demagnetization procedure itself (e.g. single axis versus three axial, static sample versus tumbling sample, field decay rates etc.). It is clear that the starting state is a function of the procedure employed and would therefore not be consistent between alternating field (AF) procedures. Measuring a backfield curve from a state of positive saturation may lead to greater deviations from lognormality, however, the starting state can be ensured and should be independent of experimental set-up etc.

Thermal relaxation and magnetic interaction result in negatively skewed distributions. This indicates that positively skewed distributions should be interpreted along the lines of mixed mineralogy. As interaction and relaxation increase, the models shift in coercivity and in many cases require two lognormal components if a close fit of the model to the data is to be achieved.

CLG modelling is a useful rock-magnetic reconnaissance tool that provides a first-principles-approach investigation of magnetic mineralogy. It is important, however, to beware of the risk of over-interpretation of a CLG model because it appears the assumption of lognormality will not always hold. For materials that contain well separated coercivity distributions CLG will provide useful rock-magnetic information, however, strongly overlapping distributions

or very minor components must be treated with caution. One further possibility is to measure the IRM curves at a variety of temperatures and compare the CLG models to investigate the thermal relaxation properties of a sample.

For simplicity our models utilized assemblages of Stoner–Wohlfarth grains. It is still necessary to investigate the behaviour of systems that contain properties such as cubic anisotropy (although in mixed assemblages uniaxial anisotropy will rapidly dominate over cubic anisotropy, Özdemir & O'Reilly 1981), multidomain behaviour, and multicomponent mineral mixtures with strongly overlapping coercivity components. However, it is not unreasonable to suggest that such properties are most likely to cause further deviations from ideal CLG behaviour. The influence of starting states on CLG models may in the future be useful when attempting to assess the magnetic composition of a natural sample: differences between the models for IRM curves started in the virgin and AC demagnetizd states have the potential to provide important information on magnetic interaction and which region of the coercivity distribution they affect most strongly (Petrovský *et al.* 1993). Future investigations should also attempt to find more flexible distributions that can act as the basis for unmixing procedures (e.g. Egli 2003), whilst the results of numerical modelling experiments should provide information on what kind of distributions would be expected for different magnetic systems.

ACKNOWLEDGMENTS

The authors are grateful to R. Egli and E. Petrovský for constructive reviews that significantly improved the quality of the manuscript. The work was performed as part of the Research Centre Ocean Margins (RCOM) at the University of Bremen and partially funded by the European Union (EC TMR project ERBFMRXCT98-02), as part of the European Network for Mineral Magnetic Studies of Environmental Problems.

REFERENCES

Azzalini, A., 1985. A class of distributions which includes normal ones, *Scand. J. Stat.*, **12**, 171–178.

Borcia, I.D., Spinu, L. & Stancu, A., 2002. Simulation of magnetization curves with Preisach-Néel models, *J. Magn. Mangn. Mater.,* **242–245**, 1034–1037.

Borcia, I.D. & Spinu, L., 2002. A Preisach-Neel model with thermally variable variance, *IEEE Transactions on Magnetics*, **38**, 2415–2417.

Conover, W.J., 1980. *Practical Nonparametric Statistics*, John Wiley & Sons, New York, USA, p. 462.

Della Torre, E., 1966. Effect of interaction on the magnetisation of single-domain particles, *IEEE Transactions on Audio Electroacoustics*, **14**, 86–93.

Dunlop, D. J. & Özdemir, Ö., 1997. *Rock Magnetism: Fundermentals and frontiers*, Cambridge University Press, Cambridge, p. 573.

Dunlop, D.J., Westcott-Lewis, M.F. & Bailey, M.E., 1990. Preisach diagrams and anhysteresis: do they measure interactions?, *Phys. Earth planet. Int.,* **65**, 62–77.

Egli, R., 2003. Analysis of the field dependence of remanent magnetisation curves, *J. geophys. Res.,* **108 (B2)**, doi:10.1029/2002JB002023.

Eyre, J.K., 1996. The application of high resolution IRM acquisition to the discrimination of remanence carriers in Chinese loess, *Studia Geophysica et Geodaetica,* **40**, 234–242.

Grygar, T., Dedecek, J., Kruiver, P.P., Dekkers, M.J., Bezdicka, P. & Schneeweis, O., 2003. Iron oxide mineralogy in late Miocene red beds from La Gloria, Spain: rock-magnetic, voltammetric and Vis spectroscopy analysis, *Catena,* **53**, 115–132.

Hejda, P., Petrovský, E. & Zelinka, T., 1994. The Preisach Diagram, Wohlfarth's remanence formula and Magnetic Interactions, *IEEE Transactions on Magnetics*, **30**, 896–898.

Hejda, P. & Zelinka, T., 1990. Modelling of hysteresis processes in magnetic rock samples using the Preisach diagram, *Phys. Earth planet. Inter.,* **63**, 32–40.

Heslop, D., Dekkers, M.J., Kruiver, P.P. & van Oorschot, I.H.M., 2002. Analysis of isothermal remanent magnetisation acquisition curves using the expectation-maximisation algorithm, *Geophys. J. Int.,* **148**, 58–64.

Kruiver, P.P., Dekkers, M.J. & Heslop, D., 2001. Quantification of magnetic coercivity components by the analysis of acquisition curves of isothermal remanent magnetisation, *Earth planet. Sci. Lett.,* **189**, 269–276.

Kruiver, P.P., Krijgsman, W., Langereis, C.G. & Dekkers, M.J., 2002. Cyclostratigraphy and rock-magnetic investigation of the NRM signal in late Miocene palustrine-alluvial deposits of the Librilla section (SE Spain), *J. geophys. Res.,* **107 (B12)**, 2334, doi:10.1029/2001JB000945.

Kruiver, P.P., Langereis, C.G., Dekkers, M.J. & Krijgsman, W., 2003. Rock.magnetic properties of multi-component natural remanent magnetisation in alluvial red beds (NE Spain), *Geophys. J. Int.,* **153**, 317–332.

Kruiver, P.P. & Passier, H.F., 2001. Coercivity analysis of magnetic phases in sapropel S1 related to variations in redox conditions, including an investigation of the S-ratio, *Geochem. Geophys. Geosyst.*, **2**, 2001GC000181.

Néel, L., 1954. Remarques sur la theorie des proprietes magnetiques des substances dures, *Appl. Sci. Res.,* **B4**, 13–24.

Özdemir, Ö. & O'Reilly, W., 1981. High-temperature hysteresis and other magnetic properties of synthetic monodomain titanomagnetites, *Phys. Earth planet. Int.,* **25**, 406–418.

Petrovský, E., Hejda, P., Zelinka, T., Kropacek, V. & Subrt, J., 1993. Experimental determination of magnetic interactions within a system of synthetic haematite particles, *Phys. Earth planet. Int.,* **76**, 123–130.

Pfeiffer, H., 1990. Determination of anisotropy field distribution in particle assemblies taking into account thermal fluctuations, *Phys. Status. Solidi. A,* **118**, 295–306.

Preisach, F., 1935. Über die magnetische Nachwirkung, *Z. Phys.,* **94**, 277–302.

Roberts, A.P., Pike, C.R. & Verosub, K.L., 2000. First-order reversal curve diagrams: A new tool for characterizing the magnetic properties of natural samples, *J. Geophys. Res.,* **B12**, 28 461–28 475.

Robertson, D.J. & France, D.E., 1994. Discrimination of remanence-carrying minerals in mixtures, using isothermal remanent magnetisation acquisition curves, *Phys. Earth planet. Int.,* **82**, 223–234.

Shcherbakov, V. & Shcherbakova, V., 1975. About magnetostatic interaction in a set of single domain grains, *Fizika Zemli,* **9**, 101–104.

Spinu, L., Borcia, I.D., Stancu, A. & O'Connor, C.J., 2001. Time and temperature-dependent Preisach models, *Physica B,* **306**, 166–171.

Spinu, L. & Stancu, A., 1998. Modelling magnetic relaxation phenomena in fine particles systems with a Preisach-Néel model, *J. Magn. Magn. Mater.,* **189**, 106–114.

Stancu, A., 1998. Temperature- and Time-Dependent Preisach Model for a Stoner-Wohlfarth Particle System, *IEEE T. MAGN.,* **6**, 3867–3875.

Stockhausen, H., 1998. Some new aspects for the modelling of isothermal remanent magnetisation acquisition curves by cumulative log Gaussian functions, *Geophys. Res. Lett.,* **12**, 2217–2220.

Stoner, E.C. & Wohlfarth, E.P., 1948. A mechanism of magnetic hysteresis in heterogeneous alloys. *Philosophical Transactions of the Royal Society of London,* **A240**, 599–642.

Thamm, S. & Hesse, J., 1998. The remanence of a Stoner-Wohlfarth particle ensemble as a function of demagnetisation process, *J. Magn. Magn. Mater.,* **184**, 245–255.

van Oorschot, I.H.M., Dekkers, M.J. & Havlicek, P., 2002. Selective dissolution of magnetic iron oxides with the acid-ammonium-oxalate/ferrous-iron extraction technique—II. Natural loess and palaeosol samples, *Geophys. J. Int.,* **149**, 106–117.

Wohlfarth, E.P., 1958. Relations between different modes of acquisition of the remanent magnetisation of ferromagnetic particles, *J. Appl. Phys.,* **29**, 595–596.

Worm, H.-U., 1999. Time-dependent IRM: A new technique for magnetic granulometry, *Geophys. Res. Lett.,* **16**, 2557–2560.